



Hierarchical self-assembly of polydisperse colloidal bananas into a two-dimensional vortex phase

Carla Fernández-Rico^{a,1} and Roel P. A. Dullens^{a,2,3}

^aDepartment of Chemistry, Physical and Theoretical Laboratory, University of Oxford, Oxford OX1 3QZ, United Kingdom

Edited by David A. Weitz, Harvard University, Cambridge, MA, and approved July 4, 2021 (received for review April 20, 2021)

Self-assembly of microscopic building blocks into highly ordered and functional structures is ubiquitous in nature and found at all length scales. Hierarchical structures formed by colloidal building blocks are typically assembled from monodisperse particles interacting via engineered directional interactions. Here, we show that polydisperse colloidal bananas self-assemble into a complex and hierarchical quasi-two-dimensional structure, called the vortex phase, only due to excluded volume interactions and polydispersity in the particle curvature. Using confocal microscopy, we uncover the remarkable formation mechanism of the vortex phase and characterize its exotic structure and dynamics at the single-particle level. These results demonstrate that hierarchical self-assembly of complex materials can be solely driven by entropy and shape polydispersity of the constituting particles.

hierarchical self-assembly | vortex phase | colloidal bananas

Self-assembly of microscopic building blocks is a powerful route for preparing materials with predesigned structure and engineered properties (1–7). Nature provides a fascinating range of self-assembled architectures offering insight into how structural organization can emerge at different length scales (8–13). In the biological world, for instance, tobacco mosaic virus coat proteins self-organize into sophisticated capsids around viral RNA strands (11, 14). In molecular systems, lipid molecules, such as fatty acids, form a range of self-assembled structures as relevant as cell membranes and vesicles (15, 16). At the colloidal scale, a rich variety of crystals with remarkable optical properties, such as opal and other gemstones, also assemble from a range of colloidal constituents (12, 17–20). The structural complexity of self-assembled materials is typically dictated by the combination of the type of interactions between the constituent building blocks and their shape (2, 3, 5, 6). Colloids are ideal systems to independently study the role of these key parameters, as their shape and interactions can be systematically tuned and rationally designed (5, 18, 21–23).

In colloidal systems interacting solely via excluded volume interactions, the shape of the particles can already lead to the assembly of complex structures (24–28). For instance, binary colloidal crystals (25) are obtained from spherical particles, complex dodecagonal quasicrystals are formed by tetrahedrons (26), and exotic banana-shaped liquid crystals are assembled from colloidal bananas (28). Introducing complex interactions between the colloidal building blocks—on the top of their shape—leads to their assembly into hierarchical materials with structural order at multiple length scales (3, 29–31). Examples include colloidal diamond structures assembled by patchy tetrahedrons functionalized with DNA strands (20) and superlattice structures formed by octapod-like particles functionalized with hydrophobic molecules (32). The successful hierarchical self-assembly of these structures relies not only on the directionality of the particle interactions but also, on the uniformity in size of the constituent building blocks, as polydispersity typically disrupts ordering via the formation of defects (33, 34).

In this work, however, we show that a colloidal suspension of polydisperse banana-shaped particles interacting only via simple excluded volume interactions (28) self-assembles into remark-

ably ordered concentric structures, which we term colloidal vortices. At high packing fractions, these structures form a quasi-two-dimensional (quasi-2D) hierarchical material, which we term the vortex phase. Using confocal microscopy, we uncover the formation mechanism of this tightly packed phase and characterize its exotic structure and dynamics at the single-particle level.

Vortex Phase from Polydisperse Bananas

In Fig. 1, we present confocal microscopy images of polydisperse micrometer-sized SU-8 colloidal bananas in water (28) with a radius of curvature R , length L , and opening angle α (the schematic is in Fig. 1A) at low and high packing fractions ϕ . These images are taken close to the bottom wall of the sample container, where the particles have sedimented into monolayer with only a few particles above it (*SI Appendix, Fig. S11*). While at low ϕ the bananas form an isotropic phase (Fig. 1B), at high ϕ bananas self-assemble into a vortex phase (Fig. 1C). This phase has a quasi-2D nature and a two-level hierarchical structure where the individual bananas first self-organize into colloidal vortices (Fig. 1D), which then further assemble into a colloidal vortex phase (Fig. 1C). Note that our colloidal vortex phase shows a structural resemblance to vortex matter seen in liquid crystals (35, 36) and magnetic materials (37, 38) (the vortex-like orientational field formed by the long axes of the bananas is shown in Fig. 1D, *Inset*), but it does not have rotational flow properties.

Significance

Hierarchically self-assembled materials—structures with order at multiple length scales—can be found everywhere. Examples range from collagen structures in human bones to engineered photonic materials. These structures usually assemble from monodisperse microscopic building blocks that interact via complex directional interactions. In this work, we show that hierarchical materials can, in fact, also be assembled from polydisperse building blocks and by entropic interactions alone. Our simple yet powerful assembly mechanism opens up avenues toward rationally exploiting the often undesired polydispersity of colloidal building blocks for programming entropy-driven self-assembly of hierarchical materials.

Author contributions: C.F.-R. and R.P.A.D. designed research; C.F.-R. performed research; C.F.-R. analyzed data; C.F.-R. and R.P.A.D. interpreted the data; and C.F.-R. and R.P.A.D. wrote the paper.

The authors declare no competing interest.

This article is a PNAS Direct Submission.

This open access article is distributed under [Creative Commons Attribution-NonCommercial-NoDerivatives License 4.0 \(CC BY-NC-ND\)](https://creativecommons.org/licenses/by-nc-nd/4.0/).

¹ Present address: Laboratory of Soft and Living Materials, Department of Materials, ETH Zurich, 8093 Zurich, Switzerland.

² Present address: Institute for Molecules and Materials, Radboud University, 6525 AJ Nijmegen, The Netherlands.

³ To whom correspondence may be addressed. Email: roel.dullens@ru.nl.

This article contains supporting information online at <https://www.pnas.org/lookup/suppl/doi:10.1073/pnas.2107241118/-/DCSupplemental>.

Published August 13, 2021.

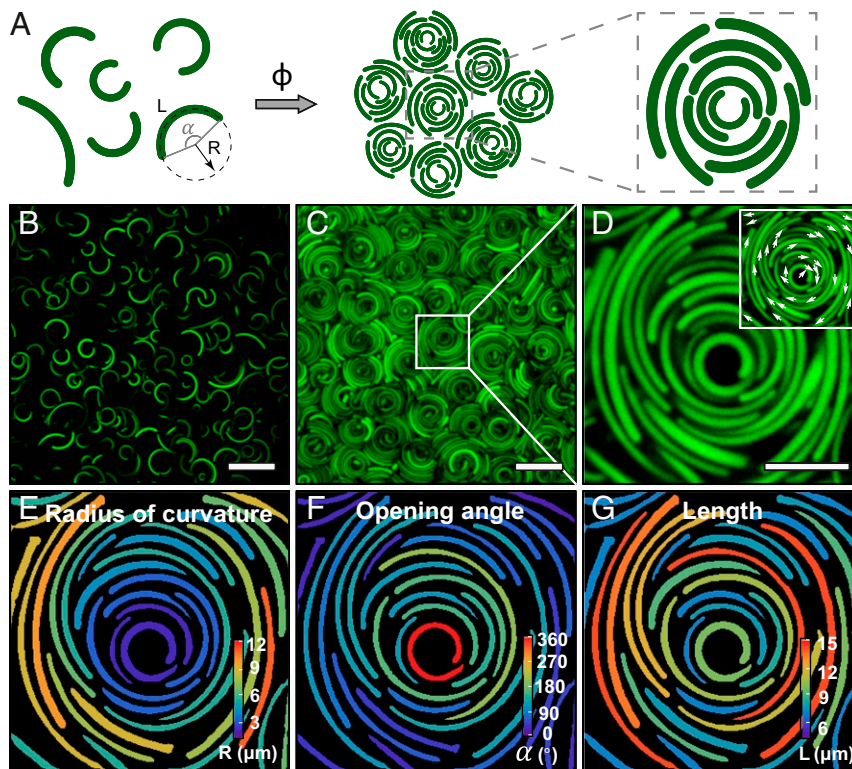


Fig. 1. Colloidal vortices from polydisperse banana-shaped particles. (A) Schematic showing the formation of colloidal vortices from polydisperse banana-shaped particles with a radius of curvature R , length L , opening angle α , and packing fraction ϕ . (B) Confocal microscopy images of (D) a dilute sample ($\phi = 0.05$) and (C) a concentrated sample of polydisperse bananas ($\phi = 0.70$) showing the hierarchical assembly of colloidal vortices. (D) Zoomed-in view of a single colloidal vortex. *Inset* shows the orientational field (white arrows) of the long axes of the bananas. (E–G) Image of a colloidal vortex where the bananas are colored according to their (E) radius of curvature, (F) opening angle, and (G) length as indicated in the legend bars. (Scale bars: B and C, 10 μm ; D, 5 μm .)

As seen in Fig. 1D, colloidal bananas within a vortex show concentric assembly where the radius of curvature of the particles increases with their radial position from the center of the vortex. This is quantified in *SI Appendix, Fig. S1* and is also evident from Fig. 1E, where the particles are colored according to their radius of curvature. A strong radial dependence is also observed in the opening angle (Fig. 1F and *SI Appendix, Fig. S1*), as bananas with a high α tend to be located closer to the center of the vortex; however, no substantial relation is found between the particle length and the radial position, as shown in Fig. 1G and *SI Appendix, Fig. S1*.

Role of Curvature and Opening Angle

To unravel the effect of curvature and opening angle on the structural formation of the colloidal vortices and the vortex phase, we prepare mixtures of two populations of polydisperse bananas with similar average lengths ($L \approx 12 \mu\text{m}$) but significantly different curvatures and opening angles, as shown in the schematics in Fig. 2. Then, we systematically change the compositions of the mixtures in order to carefully tune their R and α -distributions. Population A has a mean radius of curvature of $R_A = 6.1 \mu\text{m}$ with a mean opening angle of $\alpha_A = 140^\circ$, and population B has $R_B = 12.9 \mu\text{m}$ with $\alpha_B = 70^\circ$ (the distributions are shown in Fig. 2F and G and *SI Appendix, Fig. S3*). Note that the polydispersities in curvature, opening angle, and length are, respectively, $\sigma_R \approx 40\%$, $\sigma_\alpha \approx 50\%$, and $\sigma_L \approx 40\%$ for both populations. In Fig. 2A₁–E₁, we show confocal images of mixtures at similar overall packing fractions of $\phi \approx 0.7$ but different compositions, expressed as the number fraction of bananas from population B, x_B . Notably, we observe that while vortex phases form at low x_B (Fig. 2A₁ and B₁), mixtures

of vortices and liquid crystalline (LC) order form at intermediate x_B (Fig. 2C₁ and D₁), and only LC structures, in this case the splay-bend nematic phase (28), form as x_B approaches unity (Fig. 2E₁).

We next address the role of the particle curvature on the structural formation of these phases by measuring the overall curvature distributions of the bananas in all the mixtures (*SI Appendix, Fig. S4*) and by characterizing their local arrangement via coloring the bananas according to their curvature (Fig. 2A₂). First, we observe the characteristic assembly of the bananas into curvature-sorted concentric structures in those samples with $x_B = 0$ to 0.85 (Fig. 2A₂ and D₂). Interestingly, we find that the radius of the vortices, R_V , increases from 7.1 to 17.2 μm as x_B increases from 0 to 0.85, as shown in Fig. 2H (*SI Appendix* has details of R_V measurements). This is consistent with the fact that the fraction of bananas with large average radii of curvature (R_B), and hence, those that are typically located at the outer part of the vortices delineating their size, also increases with x_B . Accordingly, we find that R_V is roughly proportional to the mean radius of curvature of all the bananas in the mixture, R , especially at low x_B (Fig. 2H). However, the discrepancy between R_V and R increases at higher x_B as R_V seems to be highly sensitive to the fraction of particles with large radius of curvature. Remarkably, the size polydispersity of the vortices ($\sim 15\%$) is $\sim 60\%$ lower than that of the individual bananas ($\sim 40\%$), which is inherent to the single vortices being able to accommodate multiple particle curvatures. Similar size polydispersity reductions have been seen in other polydisperse systems as a result of self-assembly processes (e.g., refs. 39 and 40). We also note that at high x_B (Fig. 2D₂ and E₂), where the bananas mostly self-assemble into a splay-bend nematic phase (28), the particles with larger radius

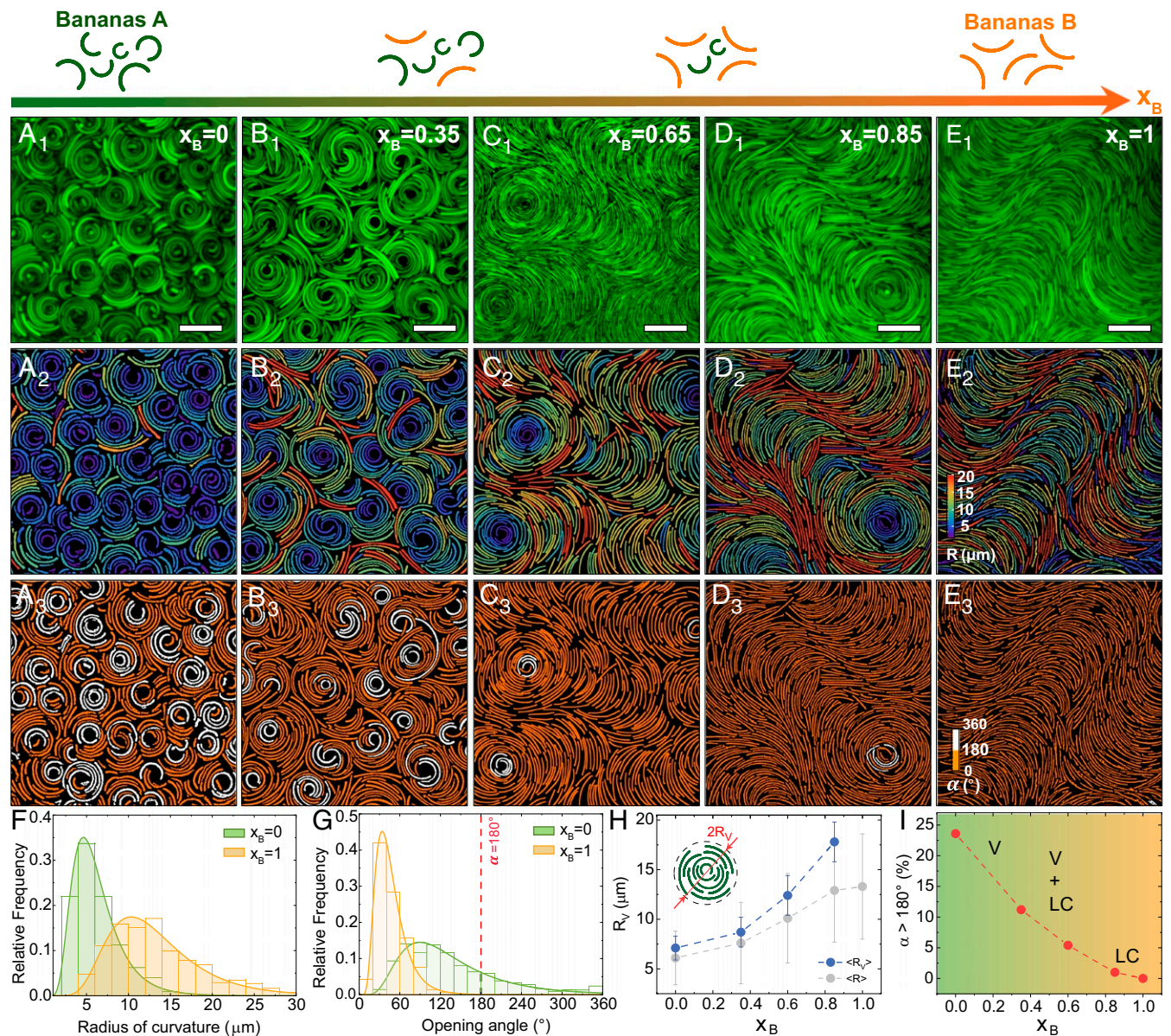


Fig. 2. Role of curvature and opening angle in the formation of vortex phases. (A_1 – E_1) Confocal microscopy images of mixtures of polydisperse bananas at a packing fraction $\phi \approx 0.7$ with number fractions $x_B = 0, 0.35, 0.65, 0.85,$ and 1 , respectively. (A_2 – E_2) Bananas colored according to their radius of curvature R . (A_3 – E_3) Bananas colored according to their opening angle α being larger (white) or smaller (orange) than 180° . Distributions of the (F) radius of curvature and (G) opening angle of the original populations. (H) Mean vortex radius R_V and mean radius of curvature of all bananas R . Inset shows a sketch of a colloidal vortex and its mean radius R_V . (I) Percentage of bananas with $\alpha > 180^\circ$ as a function of the mixture number fraction x_B . (Scale bars: $15 \mu\text{m}$.)

of curvature tend to be located in the inflection point between neighboring layers of the LC phase.

While polydispersity in the radii of curvature is clearly at the heart of the assembly of the vortices and their size, it does not fully explain the transition between the vortex and the LC phase at increasing x_B . To this end, we consider the role of the opening angle in this transition by measuring the opening-angle distributions of the bananas at all x_B (SI Appendix, Fig. S4). Next, we characterize the fraction of bananas with high opening angles, which we consider to be $\alpha > 180^\circ$ (i.e., of bananas taking up more than half of a full circle). Then, we produce binarized images according to high or low α , as shown in Fig. 2 A_3 – E_3 . From these images, we observe that bananas with high α are predominantly found at the center of each vortex (Fig. 2 A_3 – C_3) and crucially, that no vortices are formed around

bananas with $\alpha < 180^\circ$ (Fig. 2 D_3 and E_3). This clearly suggests that the presence of bananas with high opening angles is key for the formation of the vortices. We measure the percentage of bananas with high α , at all compositions (Fig. 2I), and find that it decreases from 25 to 0% as x_B approaches unity. We also find that when this percentage is smaller than 10%, the system transitions from a vortex phase to a mixture of vortices and LC ordering.

Combining our results on the role of curvature and opening angle, we conclude that vortex phases form when there is a large range of radius of curvatures with a polydispersity of $\sim 40\%$ —allowing for the radial concentric ordering according to R —and a minimum of 10% of bananas with high opening angles and small radius of curvature, which act as the nuclei of the vortices. Note that at high x_B —i.e., in the absence of bananas with

high opening angles, but still in the presence of a large polydispersity in curvature—the system does no longer find the most efficient packing by forming vortices, but via the formation of $\pm 1/2$ defects in an LC environment (SI Appendix, Fig. S7). Note that the vortices can be also seen as $+1$ defects (36, 41).

Formation of the Vortex Phase and Phase Behavior of Polydisperse Bananas

Next, we follow the formation dynamics of the colloidal vortex phase in real time using confocal microscopy. We prepare samples of bananas at a composition of $x_B = 0.35$ (where the vortex phase forms) that sediment toward the bottom of the sample cell, forming a quasi-2D monolayer (SI Appendix, Fig. S11), which we image over time as shown in Fig. 3A and B.

The formation of the colloidal vortices is a complex and dynamic process where bananas with different curvatures constantly try to form different concentric configurations in order to optimize their packing (42–44) as the particle concentration increases with time (Fig. 3A and Movie S1). The out-of-plane motion of the bananas is crucial for allowing the particles to reconfigure and find the right curvature matching the one of the already formed vortex (SI Appendix, Fig. S9 and Movie S1). As the packing fraction increases, new vortices continue to form and simultaneously self-assemble into the vortex phase (Fig. 3B and Movie S2). We observe that the typical timescale associ-

ated with the formation of single vortices is on the order of few hours, whereas their hierarchical self-assembly into a vortex phase takes place over tens of hours, clearly showing the two-step hierarchical nature of the formation of a vortex phase.

To systematically study the phase behavior of the colloidal vortices as a function of the packing fraction ϕ , we prepare concentrated samples at a fixed composition of $x_B = 0.35$. Then, we equilibrate them using a small tilt angle to induce a gradient in ϕ and hence, access multiple packing fractions using a single sample. In Fig. 3C, we show confocal microscopy images of the system at different ϕ , where the bananas are colored according to their curvature (SI Appendix, Fig. S10 shows images at all ϕ). While the bananas show isotropic ordering (I) at low packing fractions (Fig. 3C₁), above $\phi = 0.28$ they start to locally self-assemble into colloidal vortices exhibiting isotropic–vortex coexistence ($I - V$), as shown in Fig. 3C₂. Note that we use custom-written image analysis routines to identify the assembly of the bananas into vortices, which are discussed in SI Appendix (SI Appendix, Fig. S6). Around $\phi = 0.59$, the majority of the bananas self-assemble into vortices, forming the vortex phase (V) (Fig. 3C₃ and C₄). This is corroborated by the increase of the fraction of bananas in vortices as a function of ϕ (Fig. 3D), clearly showing the two main phases observed in this system. To further characterize these, we quantify the number of vortices, N_V ; the number of bananas per vortex, N_B/V ; and their radii,

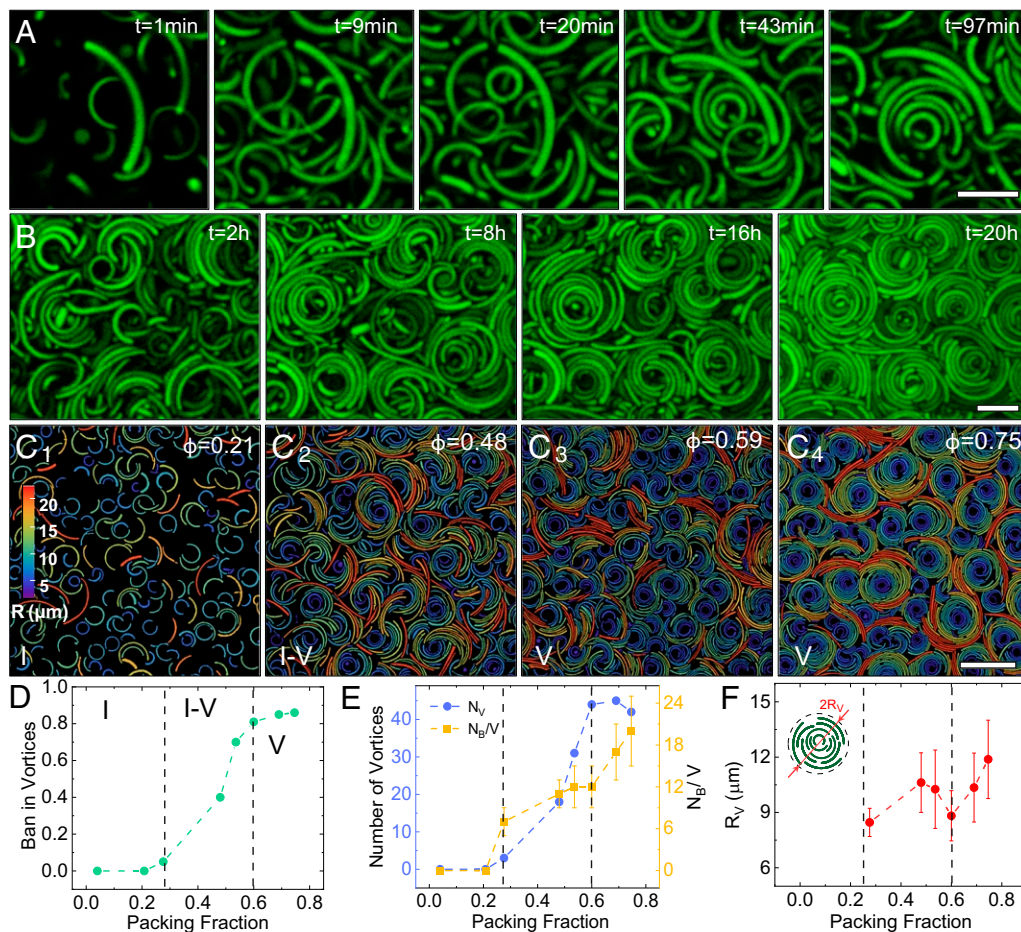


Fig. 3. Formation and phase behavior of colloidal vortices. Confocal images of (A) the formation of a single colloidal vortex and (B) the hierarchical self-assembly of vortices into the vortex phase at different times, t , after the sample preparation at $x_B = 0.35$. (C) Confocal images colored according to curvature at packing fractions ranging from $\phi = 0.21$ to $\phi = 0.75$. (D) Fraction of bananas in vortices as a function of ϕ . (E) Number of vortices, N_V , and number of bananas per vortex, N_B/V , as a function of ϕ . (F) Average size the vortices, R_V , as a function of ϕ . Inset shows a sketch of a colloidal vortex and its mean radius R_V . (Scale bars: A and B, 10 μm ; C, 20 μm .)

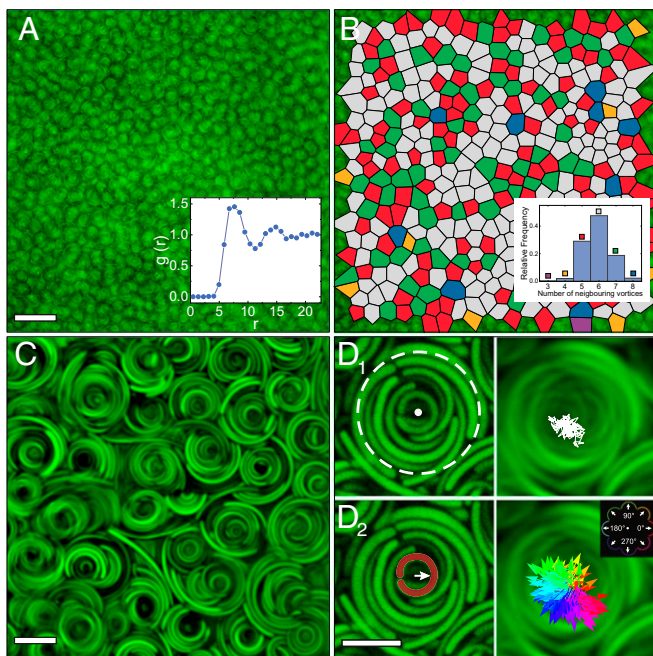


Fig. 4. Structure and dynamics of the colloidal vortex phase. (A) Large field of view confocal microscopy image of the vortex phase. *Inset* shows its radial distribution function $g(r)$. (B) Voronoi plot of the vortex phase, where the cells are colored according to the number of neighboring vortices. *Inset* shows the histogram of the number of nearest neighboring vortices. (C) Averaged confocal time series over 60 min. (D₁) Tracking of the center of mass of a single vortex in the vortex phase and (D₂) tracking of the short-axis orientation (colored arrows) of a single banana in a vortex. (Scale bars: A and B, 25 μm ; C, 10 μm ; D, 5 μm .)

R_V , as a function of the packing fraction, as shown in Fig. 3 D–F (*SI Appendix*). In the coexistence region ($\phi = 0.28$ to 0.59), the number of vortices increases proportionally with ϕ , while the number of bananas per vortex plateaus (Fig. 3E), which suggests that bananas self-assemble into vortices but still have space to reconfigure. We also measure an initial increase of the size of the vortices with ϕ , followed by a slight decrease, as the vortices are simply being compressed by the increasing density of vortices in the sample. In the vortex phase ($\phi > 0.59$), most of the bananas are forming vortices, and these just grow in size with increasing ϕ . This is shown by the roughly constant number of vortices ($N_V \approx 40$) and the increase in the number of bananas per vortex up to $N_B/V \approx 20$ (Fig. 3E) and vortex size up to 12 μm (Fig. 3F) as ϕ reaches 0.75.

Structure and Dynamics of the Vortex Phase

Finally, we characterize the structure and dynamics of the vortex phase at the vortex and single-particle level as shown in Fig. 4. First, we demonstrate that vortex phases form over large length scales as shown in the large field of view confocal microscopy image in Fig. 4A. From this image, we calculate the radial distribution function, $g(r)$ (Fig. 4A, *Inset*), and the Voronoi construction (Fig. 4B) of the vortex phase using the center of mass coordinates of the constituent vortices. The appearance of the $g(r)$ is characteristic of that of a liquid-like structure with short-range correlations only, which is consistent with the absence of significant long-range ordering of the vortices shown by the Voronoi plot and a broad distribution of nearest neighbors (Fig. 4B). We also note that the liquid-like structure of the vortex phase is consistent with the fact that the vortices are polydisperse in size ($\sim 15\%$) (45).

Lastly, we characterize the dynamics of the vortex phase by taking snapshots of its structure over time. Fig. 4C shows an

average image of the vortex phase over 60 min and qualitatively reveals that the vortices are not very mobile in the vortex phase as their structure can still be fairly well resolved after a relatively long time. This is quantified by tracking the center of mass of a single vortex in the vortex phase (Fig. 4D₁), from which we extract an approximate diffusion coefficient of $D_V \sim 0.3 \text{ nm}^2/\text{s}$ (*SI Appendix* has D_V measurements). The small D_V value is not surprising as vortices are large and complex “compound particles” moving in a highly packed environment ($\phi \sim 0.7$). Also, we note that the measured mean square displacement (*SI Appendix*, Fig. S12) appears subdiffusive at larger lag times, which could suggest a glassy nature of the vortex phase (46). Interestingly, we find that while individual bananas are radially confined in the vortices, these are actually mobile in the azimuthal direction as inferred from the large span of colored arrows representing the orientation of the short axis of the bananas (Fig. 4D₂ and *SI Appendix*, Fig. S13). In other words, this qualitatively confirms the entropy-driven assembly of the colloidal bananas into vortices at high packing fractions, as the bananas seem to maximize their azimuthal degrees of freedom at the expense of their radial free volume (42, 43, 47).

Conclusions and Outlook

In summary, we have shown that polydisperse colloidal bananas interacting only via simple excluded volume interactions can lead to the hierarchical self-assembly of banana particles into colloidal vortices, which then further assemble into a quasi-2D vortex phase with liquid-like structure. We demonstrate that both the size and number of vortices can be controlled by tuning the geometrical features of the constituent colloidal bananas, such as their curvature and opening angle. These results provide a stimulating example as to how polydispersity can be actually crucial for generating ordering across multiple length scales. As such, with our results we open avenues toward rationally exploiting the often undesired polydispersity of colloidal building blocks for programming entropy-driven self-assembly of functional materials with predesigned structure. In addition, we foresee many opportunities for further studies including, for instance, the extension of the vortex phase into the third dimension, the effect of the particle size distributions on the structure of the phases, and the nucleation of vortices using spherical particles. All of these studies will provide further insight into the self-assembly of complex structures at the colloidal scale.

Materials and Methods

Synthesis of Colloidal SU-8 Bananas. The colloidal SU-8 banana-shaped particles were prepared according to the procedure described in ref. 28. First, long SU-8 rods were synthesized via shear-flow mixing of an emulsion of SU-8 droplets in glycerol. The resulting rods were partially cross-linked by means of ultraviolet (UV)-light exposure for 30 min. In order to induce the deformation of the rods into bananas, rods were subsequently heated in a 95 °C oven for another 30 min. Finally, the banana-shaped particles were fully cross-linked via a long exposure to UV light for 60 min. The resulting colloidal bananas were transferred to water containing 0.5% Pluronic F-108. More details about the procedure are given in *SI Appendix*.

Confocal Imaging of Vortex Phases. To study the assemblies formed by our colloidal bananas, we filled rectangular VitroCom capillaries (0.1 mm \times 0.2 mm \times 5 cm) with aqueous dispersions of SU-8 bananas with an initial volume fraction of $\phi \sim 0.1$, which we subsequently sealed using epoxy glue. The colloidal SU-8 bananas slowly sedimented toward the bottom of the sample cell, forming a quasi-2D monolayer, where the imaging was performed. Note that samples were typically equilibrated for at least a week prior to imaging. A small tilt of 2° to 3° was used during the equilibration time in order to induce a small packing fraction gradient along the capillary, which enabled the concentration-dependent phase behavior studies using a single sample.

Confocal microscopy images with a 16-bit pixel depth were acquired using a 12-kHz resonant scanner head (Thorlabs) and a 532-nm laser, coupled to an Olympus IX73 inverted microscope equipped with a 60 \times (1.42 numerical aperture) oil immersion objective (Olympus).

Image Analysis from Confocal Images. The radius of curvature, length, and opening-angle distributions of the colloidal SU-8 bananas were determined by measuring the radius of curvature, length, and opening angles of at least 200 particles from the confocal microscopy images using the custom-written image analysis routines in Mathematica described in *SI Appendix*. The polydispersity (percentage) of the particles is defined as $\sigma_i = \delta_i / \langle i \rangle$, where δ_i is the SD and $\langle i \rangle$ is the mean value.

The number of vortices, the number of particles per vortex, and the vortex size were extracted by using a cluster algorithm function in Mathematica, which is described in *SI Appendix*. The packing fraction of the samples was calculated from binarized images as $\phi = N_b / N$, where N_b is the number of bright pixels corresponding to the colloidal bananas and N is the total number of pixels in the field of view. We also used custom-written image analysis routines in Mathematica to calculate the radial distribution function and the Voronoi construction of the colloidal vortices, as well as to perform the tracking of the center of mass of the vortices and the orientation and position of the individual bananas.

Scanning Electron Microscopy Characterization. The average diameter, length, and curvature of the colloidal SU-8 bananas were also determined by analyzing at least 200 particles from scanning electron microscopy (SEM) images using custom-written image analysis routines in Mathematica. SEM images were taken with a JSM-6010LV electron microscope working at 20 kV. Samples were prepared by depositing a drop of diluted aqueous particle dispersion onto a silicon chip. The solvent was evaporated using a heat lamp. Prior to the imaging, a thin layer of palladium was deposited on the sample using a Quorum SC7820 Sputter Coater.

Data Availability. All study data are included in the article and/or supporting information.

ACKNOWLEDGMENTS. We thank Adam Edward Stones for assistance with the radial distribution function measurements, Justin-Aurel Ulbrich for assistance with the particle tracking, Jeffrey Urbach for critically reading the manuscript, and Taiki Yanagishima for useful discussions. European Research Council Consolidator Grant 724834 (OMCIDC) is acknowledged for financial support.

- G. M. Whitesides, B. Grzybowski, Self-assembly at all scales. *Science* **295**, 2418–2421 (2002).
- S. C. Glotzer, M. J. Solomon, Anisotropy of building blocks and their assembly into complex structures. *Nat. Mater.* **6**, 557–562 (2007).
- D. Morpew, D. Chakrabarti, Programming hierarchical self-assembly of colloids: Matching stability and accessibility. *Nanoscale* **10**, 13875–13882 (2018).
- B. A. Grzybowski, C. E. Wilmer, J. Kim, K. P. Browne, K. J. M. Bishop, Self-assembly: From crystals to cells. *Soft Matter* **5**, 1110–1128 (2009).
- V. N. Manoharan, Colloidal matter: Packing, geometry, and entropy. *Science* **349**, 1253751 (2015).
- M. A. Boles, M. Engel, D. V. Talapin, Self-assembly of colloidal nanocrystals: From intricate structures to functional materials. *Chem. Rev.* **116**, 11220–11289 (2016).
- C. Hamon, S. Novikov, L. Scarabelli, L. Basabe-Desmonts, L. M. Liz-Marzán, Hierarchical self-assembly of gold nanoparticles into patterned plasmonic nanostructures. *ACS Nano* **8**, 10694–10703 (2014).
- P. Fratzl, R. Weinkamer, Nature's hierarchical materials. *Prog. Mater. Sci.* **52**, 1263–1334 (2007).
- A. R. Studart, Towards high-performance bioinspired composites. *Adv. Mater.* **24**, 5024–5044 (2012).
- A. V. Pinheiro, D. Han, W. M. Shih, H. Yan, Challenges and opportunities for structural DNA nanotechnology. *Nat. Nanotechnol.* **6**, 763–772 (2011).
- A. Klug, The tobacco mosaic virus particle: Structure and assembly. *Philos. Trans. R. Soc. Lond. B Biol. Sci.* **354**, 531–535 (1999).
- S. H. Kim, S. Y. Lee, S. Man Yang, G. R. Yi, Self-assembled colloidal structures for photonics. *NPG Asia Mater.* **3**, 25–33 (2011).
- S. Sun, C. B. Murray, D. Weller, L. Folks, A. Moser, Monodisperse FePt nanoparticles and ferromagnetic FePt nanocrystal superlattices. *Science* **287**, 1989–1992 (2000).
- R. D. Cadena-Nava *et al.*, Self-assembly of viral capsid protein and RNA molecules of different sizes. *J. Virol.* **86**, 3318–3326 (2012).
- I. A. Chen, P. Walde, From self-assembled vesicles to protocells. *Cold Spring Harb. Perspect. Biol.* **2**, a002170 (2010).
- B. Alberts *et al.*, *Molecular Biology of the Cell* (Garland Science, New York, NY, ed. 4, 2003).
- D. J. Norris, E. G. Arlinghaus, L. Meng, R. Heiny, L. E. Scriven, Opaline photonic crystals: How does self-assembly work? *Adv. Mater.* **16**, 1393–1399 (2004).
- N. Vogel, M. Retsch, C. A. Fustin, A. Del Campo, U. Jonas, Advances in colloidal assembly: The design of structure and hierarchy in two and three dimensions. *Chem. Rev.* **115**, 6265–6311 (2015).
- T. Hueckel, G. M. Hocky, J. Palacci, S. Sacanna, Ionic solids from common colloids. *Nature* **580**, 487–490 (2020).
- M. He *et al.*, Colloidal diamond. *Nature* **585**, 524–529 (2020).
- F. Li, D. P. Josephson, A. Stein, Colloidal assembly: The road from particles to colloidal molecules and crystals. *Angew. Chem. Int. Ed. Engl.* **50**, 360–388 (2011).
- H. Lin *et al.*, Clathrate colloidal crystals. *Science* **355**, 931–935 (2017).
- Y. Min, M. Akbulut, K. Kristiansen, Y. Golan, J. Israelachvili, The role of interparticle and external forces in nanoparticle assembly. *Nat. Mater.* **7**, 527–538 (2008).
- P. F. Damasceno, M. Engel, S. C. Glotzer, Predictive self-assembly of polyhedra into complex structures. *Science* **337**, 453–457 (2012).
- K. P. Velikov, C. G. Christova, R. P. A. Dullens, A. Van Blaaderen, Layer-by-layer growth of binary colloidal crystals. *Science* **296**, 106–109 (2002).
- A. Haji-Akbari *et al.*, Disordered, quasicrystalline and crystalline phases of densely packed tetrahedra. *Nature* **462**, 773–777 (2009).
- C. Fernández-Rico, T. Yanagishima, A. Curran, D. G. A. L. Aarts, R. P. A. Dullens, Synthesis of colloidal SU-8 polymer rods using sonication. *Adv. Mater.* **31**, 1807514 (2019).
- C. Fernández-Rico *et al.*, Shaping colloidal bananas to reveal biaxial, splay-bend nematic, and smectic phases. *Science* **369**, 950–955 (2020).
- H. Qiu, Z. M. Hudson, M. A. Winnik, I. Manners, Multidimensional hierarchical self-assembly of amphiphilic cylindrical block comicelles. *Science* **347**, 1329–1332 (2015).
- D. J. Lunn, J. R. Finnegan, I. Manners, Self-assembly of "patchy" nanoparticles: A versatile approach to functional hierarchical materials. *Chem. Sci.* **6**, 3663–3673 (2015).
- A. H. Gröschel *et al.*, Guided hierarchical co-assembly of soft patchy nanoparticles. *Nature* **503**, 247–251 (2013).
- K. Miszta *et al.*, Hierarchical self-assembly of suspended branched colloidal nanocrystals into superlattice structures. *Nat. Mater.* **10**, 872–876 (2011).
- S. E. Phan, W. B. Russel, J. Zhu, P. M. Chaikin, Effects of polydispersity on hard sphere crystals. *J. Chem. Phys.* **108**, 9789–9795 (1998).
- B. Li, D. Zhou, Y. Han, Assembly and phase transitions of colloidal crystals. *Nat. Rev. Mater.* **1**, 15011 (2016).
- P. J. Ackerman, J. Van De Lagemaat, I. I. Smalyukh, Self-assembly and electrostriction of arrays and chains of hopfion particles in chiral liquid crystals. *Nat. Commun.* **6**, 1–9 (2015).
- G. P. Alexander, G. G. C. Bryan, E. A. Matsumoto, R. D. Kamien, Colloquium: Disclination loops, point defects, and all that in nematic liquid crystals. *Rev. Mod. Phys.* **84**, 497–514 (2012).
- S. Mühlbauer *et al.*, Skyrmion lattice in a chiral magnet. *Science* **323**, 915 (2009).
- A. K. Yadav *et al.*, Observation of polar vortices in oxide superlattices. *Nature* **530**, 198–201 (2016).
- B. Luo *et al.*, Hierarchical self-assembly of 3D lattices from polydisperse anisometric colloids. *Nat. Commun.* **10**, 1–9 (2019).
- Y. Xia *et al.*, Self-assembly of self-limiting monodisperse supraparticles from polydisperse nanoparticles. *Nat. Nanotechnol.* **6**, 580–587 (2011).
- K. Usha Deniz, Defects in liquid crystals (II). *Bull. Mater. Sci.* **10**, 61–74 (1988).
- D. Frenkel, Entropy-driven phase transitions. *Physica A* **263**, 26–38 (1999).
- G. van Anders, D. Klotsa, N. K. Ahmed, M. Engel, S. C. Glotzer, Understanding shape entropy through local dense packing. *Proc. Natl. Acad. Sci. U.S.A.* **111**, E4812–E4821 (2014).
- F. Sciortino, Entropy in self-assembly. *Riv. del Nuovo Cim.* **42**, 511–548 (2019).
- T. Kawasaki, H. Tanaka, Structural signature of slow dynamics and dynamic heterogeneity in two-dimensional colloidal liquids: Glassy structural order. *J. Phys. Condens. Matter* **23**, 194121 (2011).
- W. K. Kegel, Direct observation of dynamical heterogeneities in colloidal hard-sphere suspensions. *Science* **287**, 290–293 (2000).
- L. Onsager, The effects of shape on the interaction of colloidal particles. *Ann. N. Y. Acad. Sci.* **51**, 627–659 (1949).